energies

MDPI

Article

Eco-Friendly and Economical Solar Heater Design Using Internal Structure and Phase Change Materials

Jihu Lee, Sung-Hun Son and Kibum Kim *

Chungdae-ro 1, Seowon-gu, Cheongju-si 28644, Chungcheongbuk-do, Korea; eontak0445@gmail.com (J.L.); hundenver@gmail.com (S.-H.S.)
* Correspondence: kimkb11@chungbuk.ac.kr; Tel.: +82-43-261-2446

Abstract: Indoor heating systems currently used are highly dependent on fossil fuels; hence, it is urgent to develop a new heating system to achieve carbon zero-emission. A solar air heater is eco-friendly because it generates nearly zero greenhouse gases. In this study, a parametric study was conducted for optimizing solar air heater design applicable to indoor heating. Installing the internal structure in the solar heater changes the interior flow characteristic, resulting in the air temperature increased by about 14.2 K on average compared to the heater without the internal structure. An additional case study was carried out to optimize the ideal quantity of phase change materials (PCM) in terms of mass fraction and heat capacity for various operating conditions. An excessive amount of PCM (e.g., 66% of the storage space filled with PCM) deteriorates the performance of the air heater unless the entire PCM could be melted during the daytime. After heating, the air temperature was maintained the longest when only 33% of the internal space was filled with PCM. The solar air heater can fully replace or partly assist a conventional heater for indoor heating, and it could reduce approximately 0.6 tCO_2 per year.

Keywords: phase change materials; solar air heater; carbon dioxide; simulation

Citation: Lee, J.; Son, S.-H.; Kim, K. Eco-Friendly and Economical Solar Heater Design Using Internal Structure and Phase Change Materials. *Energies* **2021**, *14*, 7423. https://doi.org/10.3390/en14217423

Academic Editor: Adrián Mota Babiloni

Received: 8 October 2021
Accepted: 5 November 2021
Published: 8 November 2021

1. Introduction

Various heating methods (electric heaters, boiler heating, heat pumps, etc.) exist for heating inside buildings; however, all these methods are not completely free from fossil fuel use, which causes a problem of environmental pollution [1]. A new alternative energy-based heating system to solve this problem was carried out [2,3]; among them, solar air heaters with solar energy can provide unlimited power in a sunlit environment [4–6]. Solar air heaters are an eco-friendly energy system without worrying about the depletion of resources; therefore, it is possible to solve the problem of carbon dioxide (CO_2) emissions resulting from the combustion of fossil fuels in the existing heating method. In Iran, where the supply of solar energy is sufficient, replacing the carbon based fuel for the steam generator with solar heat has gained as much performance as a conventional fossil fuel generator with eco-friendly advantages [7]. Although heating is required more in cold regions or winter, it is difficult to use the solar air heater efficiently due to insufficient solar irradiance at that time around, which would be a disadvantage of using the solar air heater. The shortcomings can be minimized by enhancing the absorption agility of the sunlight and storing the heat longer.

Many studies have been performed to improve the performance and efficiency of solar air heaters. Because aluminum with high thermal conductivity is beneficial for heat transfer, aluminum structures were installed inside the heater to improve the transfer rate of solar energy, resulting in an increase in the heated air temperature by 101% of the ambient air [8]. In addition, the surface of the aluminum structure inside the heater is coated in black to facilitate solar energy absorption, improving the performance of the heater [9]. Accordingly, studies were conducted to store solar heat using phase change materials (PCM) during the daytime and to use the solar air heater for extended periods

using stored heat even in the nighttime [10,11]. Due to different melting points depending on the materials, various PCM types have been used for space heating in buildings or heat sinks of electronic devices [12]. A comparative experimental study of Packed Bed Thermal Energy Storage and PCM was conducted to investigate and analyze the maximum stored thermal energy of energy storage media [13]. Energy efficiency according to the capacity of PCM storage tanks in buildings and HVAC systems was experimentally studied, and average energy efficiency of 68.55% was obtained [14].

The performance of a solar air heater can also vary depending on the transmittance of the glass installed in the front of the solar air heater. An effort was made by applying glass with higher transmittance than ordinary glass through a study conducted on solar energy absorption according to the solar spectrum. The device absorbs about 81, 87, and 76% of infrared, ultraviolet, and visual light [15]. A research group investigated the effect of changes in the structure (e.g., the shape ratio, the angle of attack) on the performance of heaters by adding fin structures inside the heater, and they found that the highest daily efficiency of the heater increased from 32% to 57% at 0.04 kg/s [16,17]. Instead of a box-shaped solar air heater design that is ineffective for heating air inside the heater, a tubular solar air heater was fabricated using several tubes. It could raise the heated air temperature by approximately 13.2 °C more than the box-shaped one at the air mass flow rate of 0.025 kg/s [18]. The flow path inside the solar air heater was increased from the existing single to the double path to increase the heating time of the air inside the heater [19–21]. The heat transfer could also be improved by roughing the internal surface of a solar air heater [22,23]. The absorption plate of a solar air heater covered with thin porous material was another choice to improve the performance of the heater in terms of heat transfer characteristics and enhance the turbulence effect in the heater [24]. A computational study supports the fact that the performance of the solar heater is affected by the heater design. It was revealed that a curved shape of the absorption plate inside a solar air heater improves the performance and thermal efficiency of the heater [25].

Although numerous researches have been studied to increase the thermal efficiency of heaters, further research is still needed for optimal system development. To date, most studies have been conducted on the shape of flow paths, PCM, and heater size, but there have been no studies considering all at once, especially carbon dioxide reduction using solar air heaters. In this study, an analytical model of a solar heater was developed to optimize the flow path inside the heater and the quantity of PCM. In particular, the performance of a solar air heater alone is inadequate to heat the entire room in an area where solar irradiance is insufficient. However, the solar heater could play a pivotal role in supporting the existing heater use and consequently reduce CO_2 emission, which was evaluated in this study.

2. Methodology

2.1. Solar Air Heater

An experiment was conducted to investigate the performance of the designed solar air heater at a position of 36°38′ N 127°26′ E, Cheongju, Republic of Korea. Figure 1a–c show the schematic and photographs of the solar air heater used for the experiment. It consists of an internal structure changing the flow of air inside the heater, aluminum cans containing phase change materials that absorb and store heat, and a 12V DC fan to create to suck of air inside. The fan installed at the outlet allows the air inside the heater to flow at a constant flow rate, and the ambient air is sucked in naturally into the heater inlet. The glass on the front of the heater is a 4 mm thick low-iron patterned glass. Unlike ordinary glass with an iron content of between 500 and 1000 ppm, the glass contains a low-iron content of around 175 ppm, which enhances the penetration rate of solar light, making it possible that the low iron glass is suitable for use in heaters. Oriontek's solar power meter DT-1307 CEM was used to measure solar irradiance. The air temperature and wind speed out of the heater were measured using a hot air velocity meter (testo, 405i). The condition of the inlet air is under the atmospheric pressure condition of 1 atm and temperature of 304 K.

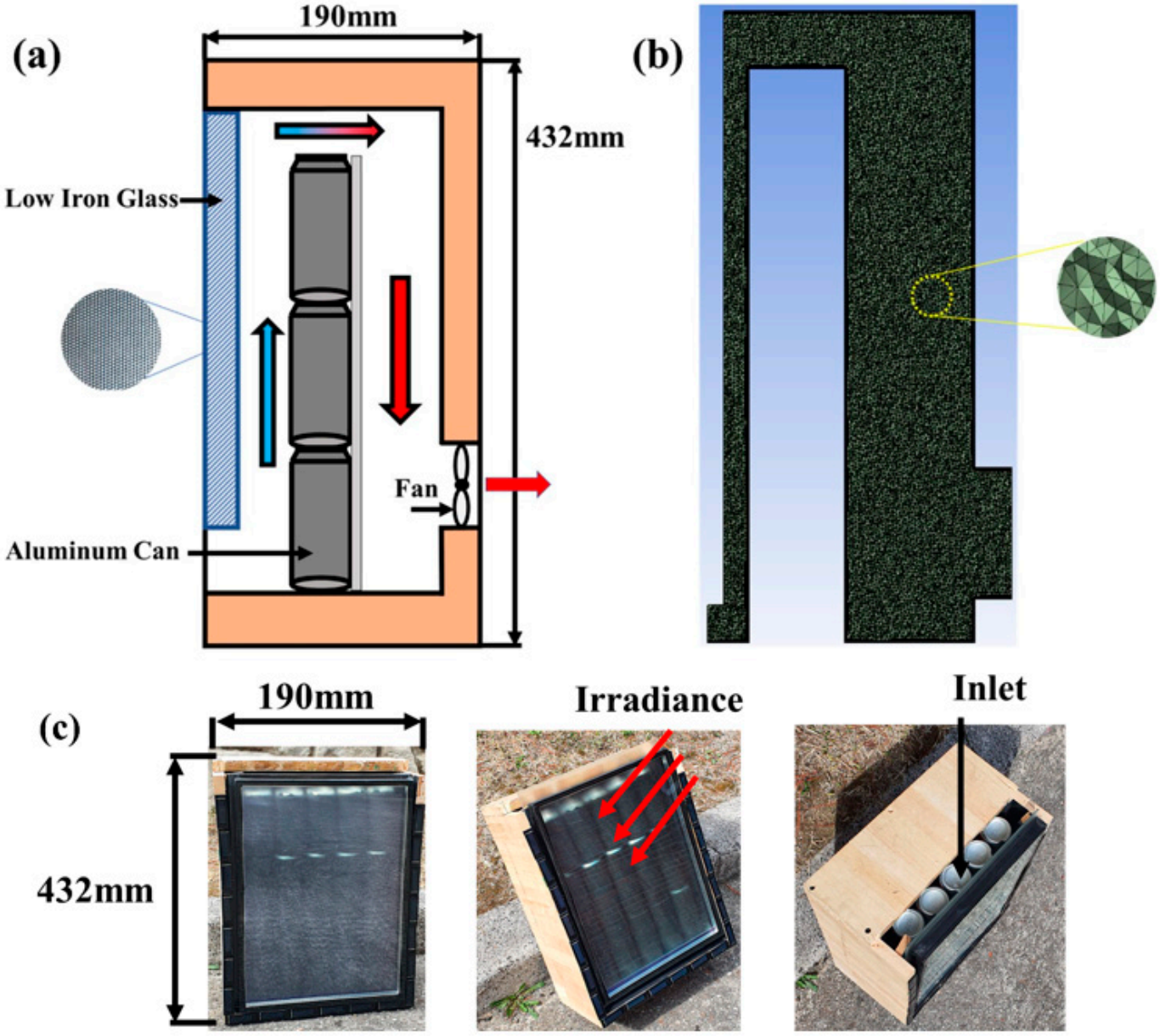

Figure 1. Solar air heater used for the experiment, (**a**) Schematic, (**b**) Tetrahedral meshes generated inside the solar heater, (**c**) Photographs of the solar air heater.

A 3D computational model was developed to investigate the performance of solar air heaters using commercial CFD software FLUENT 17.2 (ANSYS V6.3.26). Figure 1b shows the mesh generated in the computational domain. The mesh was mainly formed as a tetrahedral mesh with a total of 1,430,000 meshes created.

2.2. Theory

The rate of heat generated by the heater, $\dot{Q}$ is determined by Equation (1),

$$\dot{Q} = C\dot{m}\Delta T \quad (1)$$

where $\dot{m}$ is the mass flow rate of the air, and ΔT is the temperature difference between the air inlet and outlet. C is the specific heat of the air, which is dependent on temperature; hence, it can be calculated with Equation (2) over some temperature range.

$$C_m = \frac{1}{T_2 - T_1} \int_{T_1}^{T_2} C dT \tag{2}$$

where C_m is the average of specific heat. The following expression is used to obtain the value of m,

$$\dot{m} = A \times \rho \times u \tag{3}$$

where ρ is the density of the air, A is the area of the inlet or outlet, and u is the velocity of the airflow.

The mass and momentum conservation equations are used to calculate the flow of air as follows.

$$\frac{\partial \rho}{\partial t} + \frac{\partial}{\partial x_i}(\rho u_i) = 0 \tag{4}$$

$$\frac{\partial}{\partial t}(\rho u_i) + \frac{\partial}{\partial x_i}(\rho u_i u_j) = -\frac{\partial p}{\partial x_i} + \frac{\partial \tau_{ij}}{\partial x_j} + \rho g_i + F_i \tag{5}$$

where ρ is the density of the fluid, t is the time, u_i is the velocity of the fluid of species i, p is the static pressure, τ_{ij} is the shear stress tensor acting on fluids of plane ij, and g_i is the gravity of species i, and external force acting on F_i of species i. The formula for τ_{ij} is as follows.

$$\tau_{ij} = \left[\mu \left(\frac{\partial u_i}{\partial u_j} + \frac{\partial u_j}{\partial x_i} \right) \right] - \frac{2}{3} \mu \frac{\partial u_k}{\partial x_k} \delta_{ij} \tag{6}$$

where μ is the viscosity of air.

A standard k-ε equation using turbulent kinetic energy k and turbulent dissipation rate ε is used to interpret the turbulence intensity in a fluid. The equations are as follows:

$$\frac{\partial}{\partial t}(\rho k) + \frac{\partial}{\partial x_i}(\rho k u_i) = \frac{\partial}{\partial x_j} \left[\left(\mu + \frac{\mu_T}{\sigma_k} \right) \frac{\partial k}{\partial x_j} \right] + G_k + G_b - \rho \varepsilon - Y_M + S_k \tag{7}$$

$$\frac{\partial}{\partial t}(\rho \varepsilon) + \frac{\partial}{\partial x_k}(\rho t u_i) = \frac{\partial}{\partial x_j} \left[\left(\mu + \frac{\mu_T}{\sigma_\varepsilon} \right) \frac{\partial \epsilon}{\partial x_j} \right] + C_{1\epsilon} \frac{\partial \epsilon}{\partial x_j} (G_k + C_{3\epsilon} G_b) - C_{2\epsilon} \rho \frac{\epsilon^2}{k} + S_\epsilon \tag{8}$$

where G_k is the kinetic energy of turbulence caused by mean velocity gradient, and G_b is the kinetic energy of turbulence caused by buoyancy. $C_{1\epsilon}$, $C_{2\epsilon}$, and $C_{3\epsilon}$ are constants used for calculation. Y_M is the effect of fluctuation in the dissipation of turbulence. σ_k and σ_ε is the turbulent Prandtl number of k and ε, respectively. S_k and S_ϵ are required constants. μ_T is the synthesis of k and ε, which is expressed in the following equation:

$$\mu_T = \rho C_\mu \frac{k^2}{\epsilon} \tag{9}$$

where C_μ is constant.

Heat transfer inside solar air heaters is vital in analytical models. Thus, conduction and convection heat transfer can be expressed in the following energy equation:

$$\frac{\partial}{\partial t}(\rho E) + \nabla \cdot \left(\vec{v}(\rho E + p) \right) = \nabla \cdot \left(k_{eff} \nabla T - \sum_j h_j \vec{J}_j + \left(\overline{\overline{\tau_{eff}}} \cdot \vec{v} \right) \right) + S_h \tag{10}$$

where k_{eff} is the conduction heat coefficient, and $\vec{J}_j$ is the diffusion flux in species j. $k_{eff} \nabla T$, $\sum_j h_j \vec{J}_j$ and $\left(\overline{\overline{\tau_{eff}}} \cdot \vec{v} \right)$ are the energy exchange terms for conduction, diffusion, and

viscous dissipation, respectively. S_h is a heat or external energy term produced by a phase change reaction.

The latent heat of PCMs from solid to liquid can be calculated by

$$Q_{pcm} = m \cdot \Delta h + \int_{T_1}^{T_m} m \cdot c_p \cdot \Delta T + \int_{T_m}^{T_2} m \cdot c_p \cdot \Delta T \tag{11}$$

where m is the mass, Δh is the enthalpy change, and c_p is the specific heat of the PCMs [26]. T_1, T_2, and T_m are the initial, final, and melting temperatures, respectively.

To calculate the CO_2 emissions, LHV (Low Heating Value) of fuels is calculated as follows:

$$Q_{LHV} = F_c \times H_e \tag{12}$$

where F_c is the amount of fuel used, and H_e is the amount of heat generated. The equation for obtaining carbon emissions using CO_C is as follows:

$$CO_c = Q_{LHV} \times C_{CO} \div 10^6 \tag{13}$$

where CO_c is the carbon emission quantity, and C_{CO} is the carbon emission coefficient. The equation for calculating the amount of carbon dioxide emissions is as follows:

$$C_{CO_2} = CO_C \times \frac{44}{12} \tag{14}$$

The equation allows the calculation of carbon emission reduction by using the solar air heater compared to conventional heating devices [27].

2.3. Computational Model

Figure 2 shows a solar air heater model with different internal flow path structures. As a boundary condition, the velocity of the inlet air is 0.8 m/s, and the temperature is 278.15 K. The computational model calculates the change in temperature and velocity of the air at the outlet when the solar irradiance of 900 W/m^2 is supplied through the front windshield. Table 1 tabulates the boundary conditions for computational analysis. The different built-in structure affects the heat transfer characteristics by changing the airflow pattern and turbulence intensity. The time for the air to heat up is increased by reducing the air velocity inside the heater, and the turbulent flow enhances convective heat transfer from the inner wall of the heater to the air.

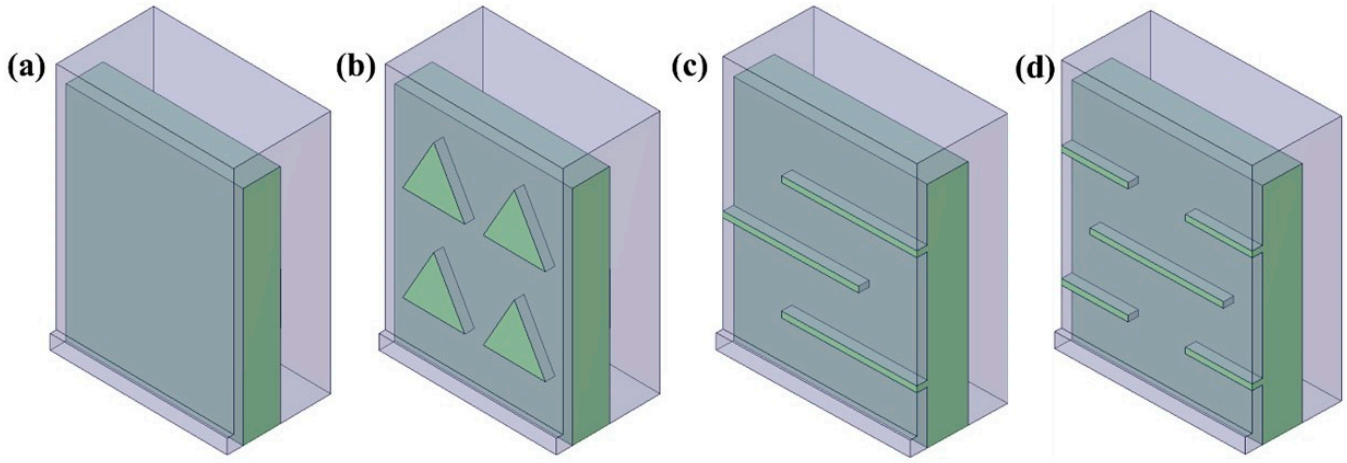

Figure 2. Four different flow paths to change internal airflow patterns. (**a**) Basic model, (**b**) Model 1, (**c**) Model 2, (**d**) Model 3.

Table 1. Boundary conditions for the computation.

Boundary conditions	Inlet velocity (m/s)	0.8
	Temperature (K)	278.15
	Solar irradiance (W/m^2)	900
Other conditions	Gravity (m/s^2)	9.81
	Turbulence	Standard $k-\varepsilon$
	Type	Steady State, Transient State
Materials	Base (W/mK)	Wood, conductivity: 0.29
	Can (W/mK)	Aluminum, conductivity: 350
	PCM (W/mK)	Paraffin Wax, conductivity: 0.24, 0.22

In addition, paraffin wax was used for the PCM inside the solar air heater. The properties of the paraffin are summarized in Table 2. The numerical study of melting of the PCM for thermal energy storage inside the heater was also performed. The melting of a rectangular PCM domain with its left side exposed to constant heat flux by the solar irradiance and the other three sides exposed to time-variant heat flux from the airflow inside the heater is simulated using ANSYS (Fluent) software. The assumptions and equations used in the numerical modeling were already discussed in the previous section. The contours of liquid fraction and temperature of PCM at regular intervals of 0.01 s are represented for a total melting time of 10,000 s. The change in the melting fraction with time is also discussed, which tells us about the percentage of melted PCM at different instants of time. Boundary conditions were set such that different amounts of PCM (e.g., 0%, 33%, 66%) were filled inside the storage in the heater, and the same amount of solar irradiance of 900 W/m^2 was received. The performance of the heater in terms of the temperature and velocity of the air through the heater outlet was evaluated while solar radiation of 900 W/m^2 was supplied into the heat absorbing plate for either 6000 s or 10,000 s. The air also enters the inlet of the heater at the temperature of 298.15 K and velocity of 0.8 m/s to investigate how much air temperature increases due to the influence of PCM on the performance of the heater and how long it is possible to store heat to maintain the temperature constant. From an economic point of view, paraffin wax is currently priced at about $0.13/kg. Therefore, the application of PCM to solar air heaters is not a big problem in economic feasibility.

Table 2. Physical property of paraffin wax [28].

Property	Solid	Liquid
Melting temperature (K)	326	
Latent heat (kJ/kg)	190	
Density (kg/m^3)	910	790
Specific heat (kJ/(kg·K))	1.82	2.17
Thermal conductivity (W/(m·K))	0.24	0.22

2.4. Optimal Modeling

In addition to the shape of the flow path, the number of obstacles and arrangement as shown in Figure 3a–c can affect the performance of the solar air heater. Moreover, the size of the heater must be optimized to use the solar air heater in practice. The optimal model of the solar air heater analyzed by the computational analysis is shown in Figure 3d. The optimal model of the solar air heater that can maintain the target room temperature of 301 K based on November in Korea through computational analysis is shown in Figure 3d. From all computational results obtained with the optimal model, the amount of carbon emission reduction was compared with that of conventional heating devices.

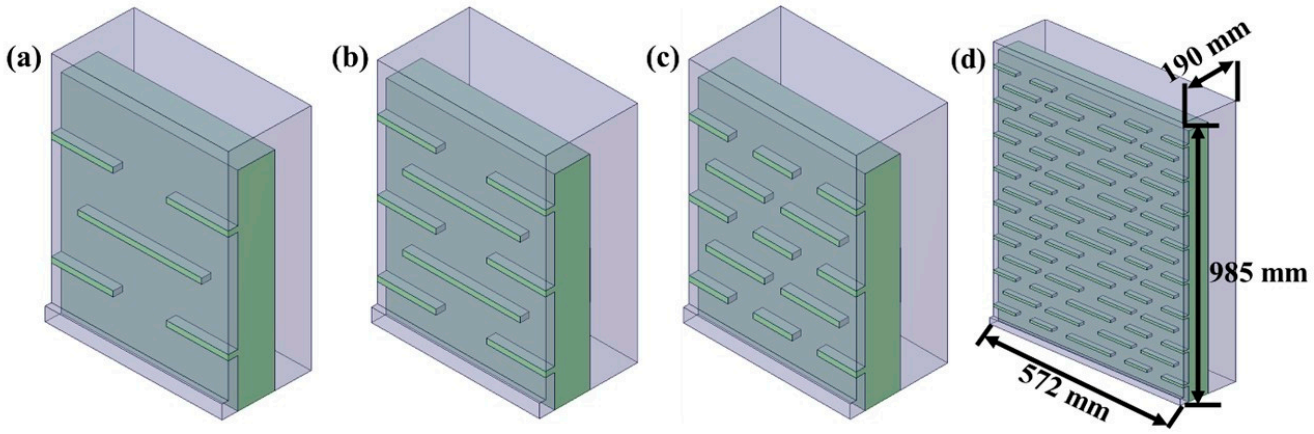

Figure 3. Optimal Flow path model (**a**) Model 3, selected based on the computational study, (**b**) Model 3-I, (**c**) Model 3-II, increased number of the flow path, (**d**) Optimal size of the solar heater with geometry.

3. Results and Discussion

3.1. Validation

Figure 4 represents experimental and computational results on the temperature of air discharged from the solar air heater. For experimental purposes, a solar air heater was installed outdoors at 10 a.m., and the air temperature from the outlet was measured every hour from 11 a.m. to 3 p.m. using a hot air velocity meter (testo, 405i). The accuracy of the experimental equipment was ±0.5 °C. In addition, the solar illuminance was checked every hour based on the Korea Meteorological Administration data of the same day, and it was used as an input parameter for computation. An uncertainty analysis was carried out for the experimental result (e.g., the air temperature at the heater outlet, T_{outlet} in Figure 4. The air temperature heated through the solar air heater is mainly dependent on two parameters such as the solar irradiance, I_{solar} and the ambient temperature, T_{amb}. Based on the experimental data, the air temperature could be expressed using an empirical equation.

$$T_{outlet} = 0.065 \cdot {I_{solar}}^{0.75} + T_{amb} \tag{15}$$

and then the uncertainty can be determined as below,

$$\sigma_{T_{outlet}} = \sqrt{\left(\frac{\partial T_{outlet}}{\partial I_{solar}}\right)^2 \cdot {\sigma_{I_{solar}}}^2 + \left(\frac{\partial T_{outlet}}{\partial T_{amb}}\right)^2 \cdot {\sigma_{T_{amb}}}^2} \tag{16}$$

The overall uncertainty values for T_{outlet} are 1.66, 1.85, 181, 1.4, and 1.61 °C for five different times.

When comparing the experimental results and the analysis results, values fall within a relative error of about 1%, confirming the reliability of the computational model. Based on the validation for the model, a case study was conducted using the model with confidence.

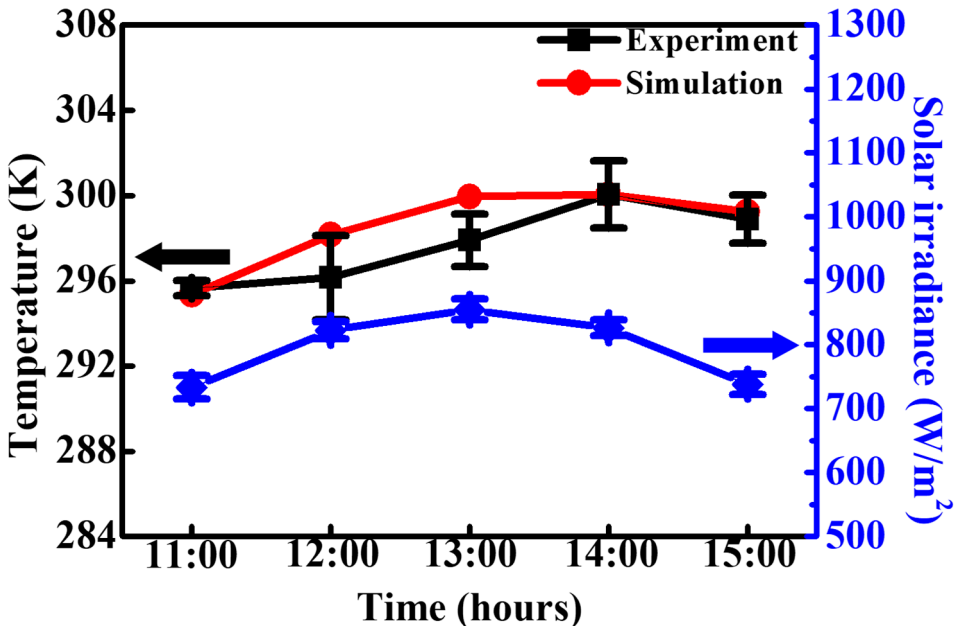

Figure 4. Temperature of discharged air from the solar air heater was measured during a typical sunny day in April in South Korea and compared with simulation results.

3.2. Case Study

3.2.1. Flow Path

When checking the winter temperatures in South Korea over the past ten years, the maximum temperature is about 278.15 K, and the average temperature is about 273.15 K. Since the solar air heater receives heat during the daytime when the sun rises, the analysis conditions were selected based on the maximum temperature in winter, 278.15 K. It was accessed that the influence of the change in the internal structure of the solar air heater under the inlet conditions: the air temperature of 278.15 K and the velocity of 0.8 m/s. Figure 5 shows the air velocity distribution forming in the front flow path of the heater for various internal structures. Changes in velocity and turbulence intensity are attributed to the differences in flow path structures that affect the amount of solar energy absorbed by the heater. It was noted that the air velocity inside the heater reached up to 11 m/s in Model 2 because the cross-sectional area of the path decreased more than ten folds. Model 1, 2, and 3 show an increase in temperature of 12.65 K, 14.28 K, and 14.2 K compared to the inlet temperature, respectively. The flow path of Model 1 does not change the airflow significantly, so the temperature increase with the internal structure is relatively small. The maximum air temperature is no significant difference between Model 2 and 3; however, Model 3 is a more efficient flow path design since the air reaches the maximum temperature sooner (Figure 6a).

The previous analysis concluded that Model 3 is the most effective design to help quickly reach the steady-state air temperature. While the shape of the flow path is maintained, the number of the inner flow path is increased, as shown in Figure 3. Figure 6b shows the air temperature change for the different numbers of the internal flow path. The effect of the number of the inner flow path is trivial on the maximum air temperature at the outlet of the heater. Based on the above results, the optimal size for the heater was determined (Figure 3d).

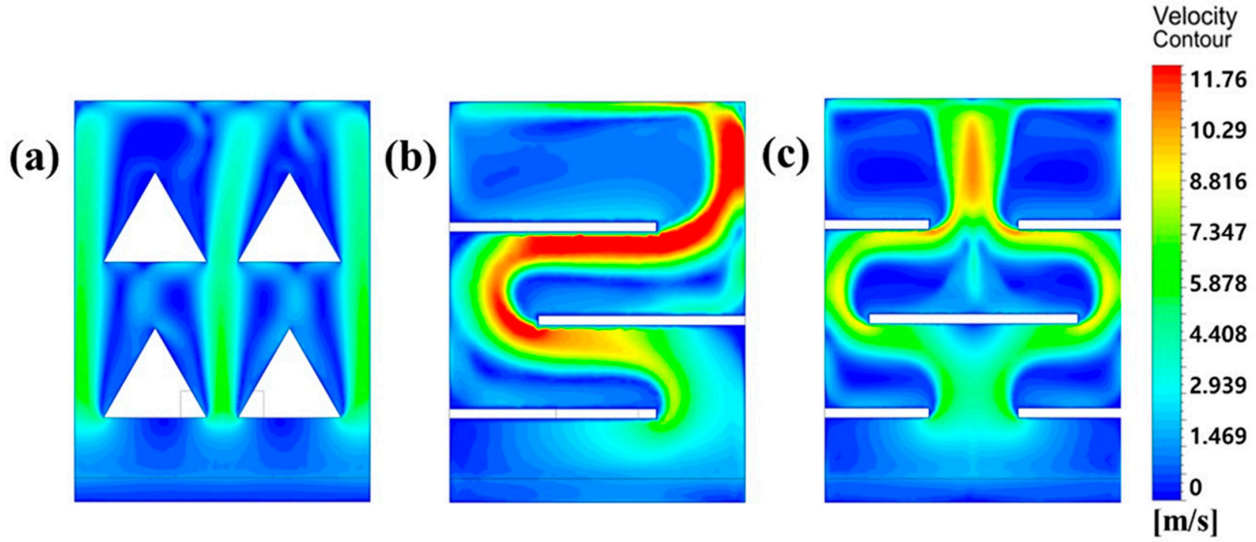

Figure 5. Airflow velocity distribution of solar air heater. (**a**) Model 1, (**b**) Model 2, (**c**) Model 3.

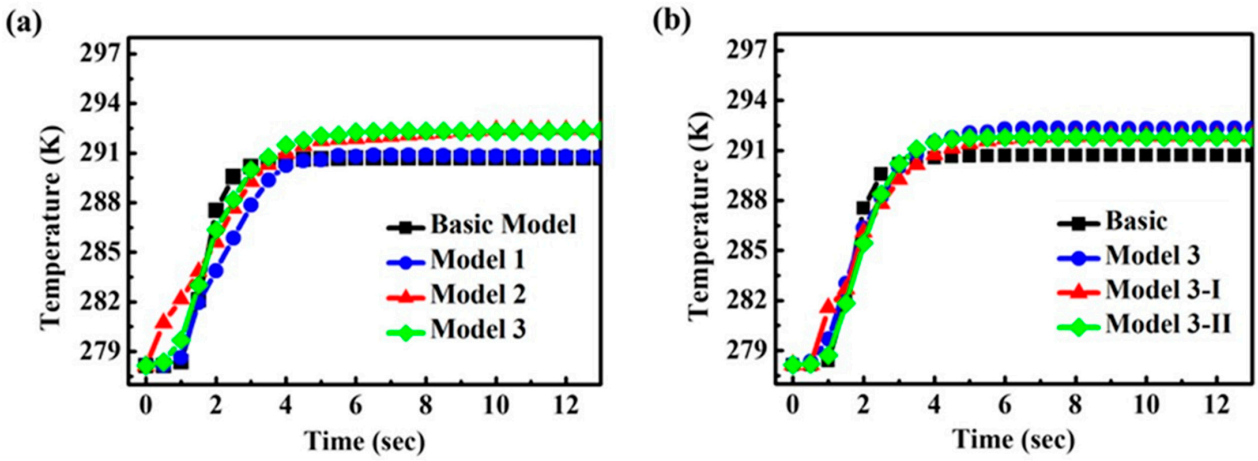

Figure 6. Temperature change for each model according to (**a**) different flow path shapes, (**b**) different number of flow paths.

The average room size in Korea is normally 15 m^2, and the heating capacity of 3435.15 kJ/h is required for heating the room since the heat capacity needed to heat an area of 1 m^2 is 229.01 kJ/h [29]. The indoor temperature should be steadily maintained at 301.15 K, which is the typical temperature that people feel most comfortable with based on dry-bulb temperature. Heat loss through doors, windows, and walls occurs steadily due to outside temperatures lower than indoors. The average heat loss of buildings in South Korea during the winter season is approximately 37%. With the assumption, the optimal heater size (Figure 3d) was determined to increase outlet air temperature by 36.52 K to 314.67 K at the outlet when 278.15 K was given at the inlet. Specific heat of the air is calculated as a function of temperature with a mass flow of 0.0413 kg/s. The heat capacity that can be supplied from the solar air heater under this condition about 5456.943 kJ/h, which is a heat capacity capable of maintaining the indoor target temperature (301.15 K) in consideration of a steady heat loss of 37%. Since the solar irradiance varies from month to month, the outlet temperature also changes, and it significantly decreases in the middle of winter compared to fall and spring. Therefore, more fan power should be needed to increase the mass flow rate of the air through the solar heater. Figure 7 indicates the maximum temperature for indoor heating and expected outlet temperature from heater varying due to different outdoor ambient temperatures and solar irradiance from month to month. Therefore, insufficient heat should be replenished using conventional heating

equipment to raise the air temperature to the target temperature (~301 K) or consuming more power for operating the fan.

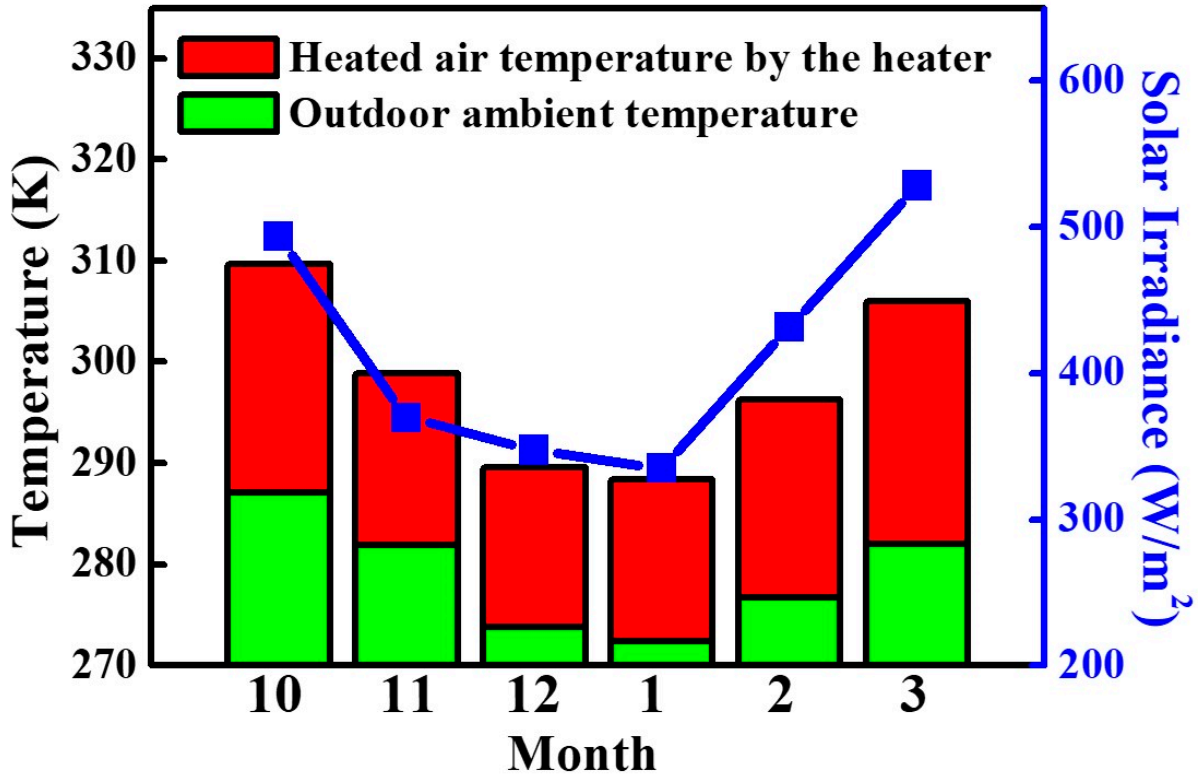

Figure 7. Maximum indoor heating temperature and heater outlet temperature according to monthly irradiance.

3.2.2. Phase Change Material

Heat storage capacity of the solar heater according to PCM charging rate of 0%, 33%, 66% in the storage inside the heater was analyzed using the computational model. Figure 8 shows the discharging air temperature at the heater outlet for each case. Initially, the solar irradiance was supplied for 6000 and 10,000 s through the front window of the heater and then blocked the sunlight. In the case of a heater using 33% PCM to store thermal energy, the solar irradiance for 6000 s is not sufficient for the temperature of the heated air to reach a steady state. The heat was used for the endothermic reaction of PCM rather than heating the air. However, supplying the solar irradiance for 10,000 s rises until the air temperature reaches a steady state in all cases since the phase change of PCM is completed regardless of the charging rate of PCM. If the solar energy is cut off after 10,000 s, the air temperature will drop to 302 K after 406 s for 0%, 15,681 s for 33%, and 8595 s for 66%, depending on the case.

In opposite to the idea that more PCM is advantageous to store heat, the air temperature is higher when 33% of the storage space was filled with PCM, and the temperature is maintained for a relatively long time. Figure 9 shows that 60% and 40% of the PCM filled in the storage tank was melted when the PCM charge was 33% and 66%, respectively, after 10,000 s of solar energy supply of 900 W/m^2. The amount of solar radiative heat absorbed is insufficient to melt the PCM fully for 10,000 s. Although the heat storage capacity increases with the higher amount of PCM, it causes the delay time of raising the temperature and changing phase of the material. Therefore, the in energy storage and maintaining higher air temperature longer than the case of 66case of 33% shows a higher percentage of PCM melt, thereby showing better performance%. However, once the solar irradiance of 900 W/m^2 is absorbed over 4 h, the PCM keeps melting, and the performance of the 66% case would

finally become better. Care must be taken to select an appropriate amount of PCM based on the user environment (e.g., location, seasons).

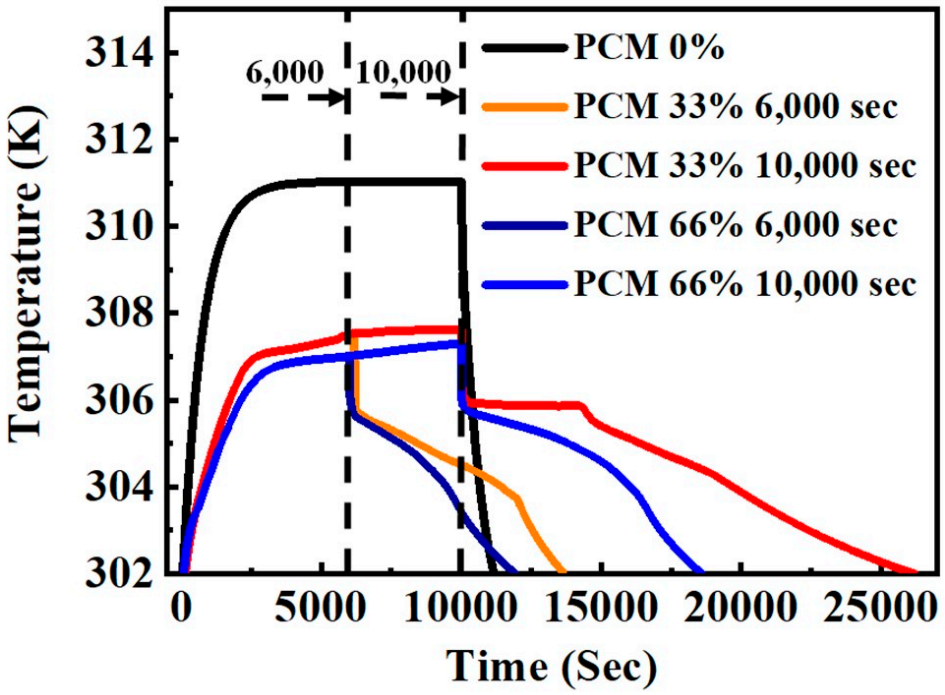

Figure 8. Air temperature change for different PCM quantities during a certain period under the constant solar irradiance of 900 W/m^2.

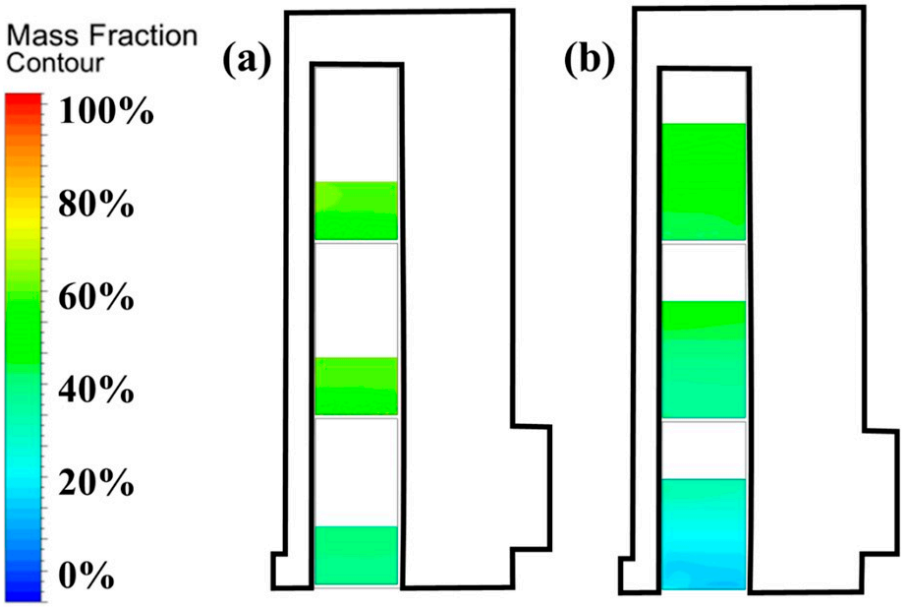

Figure 9. PCM melting rate when the solar irradiance of 900 W/m^2 is supplied for 10,000 s. (**a**) 33%, (**b**) 66% PCM charged in storage.

3.2.3. Carbon Dioxide Reduction

As shown in Figure 7, the different solar radiation affects the solar air heater performance varying from month to month. The performance of the heater can be maintained by changing the fan power of the heater. From October to February, the indoor air temperature according to the fan power of the heater is summarized in Table 3. It is noted

that in October, November, and March, solar air heaters alone can supply sufficient heat to maintain an indoor target temperature of 301 K without additional heat supply through fossil fuel combustion. However, the solar air heater cannot provide enough heat for indoor heating in December, January, and February due to the lack of solar irradiance. Additional heat must be required to maintain the indoor temperature of 301 K. Figure 10 shows the amount of CO_2 generated using a conventional heater by consuming fossil fuels such as coal, light diesel, propane, and methane [30]. The CO_2 emissions from conventional heating equipment are as follows: coal is 0.03191 tCO_2, light diesel is 0.144312 tCO_2, propane is 0.122882 tCO_2, and methane is 0.109308 tCO_2. The CO_2 emission can be significantly reduced with the solar air heater, and a small amount of CO2 is only generated by the operating fan of the solar air heater. If the electricity could be produced with photovoltaic cells, zero CO_2 emission would be achieved in October, November, and March.

Table 3. From October to February, the indoor air temperature according to the fan power of the heater.

	October	November	December	January	February	March
Power (W)			**Indoor Temp (K)**			
2938.776	314.497	303.654	294.401	293.144	301.113	310.854
1469.388	314.379	303.491	294.169	292.9	300.906	310.691
293.878	313.43	302.185	292.309	290.944	299.244	309.393
146.939	312.244	300.554	289.983	288.498	297.167	307.77
29.3878	302.754	287.501	-	-	280.551	294.786

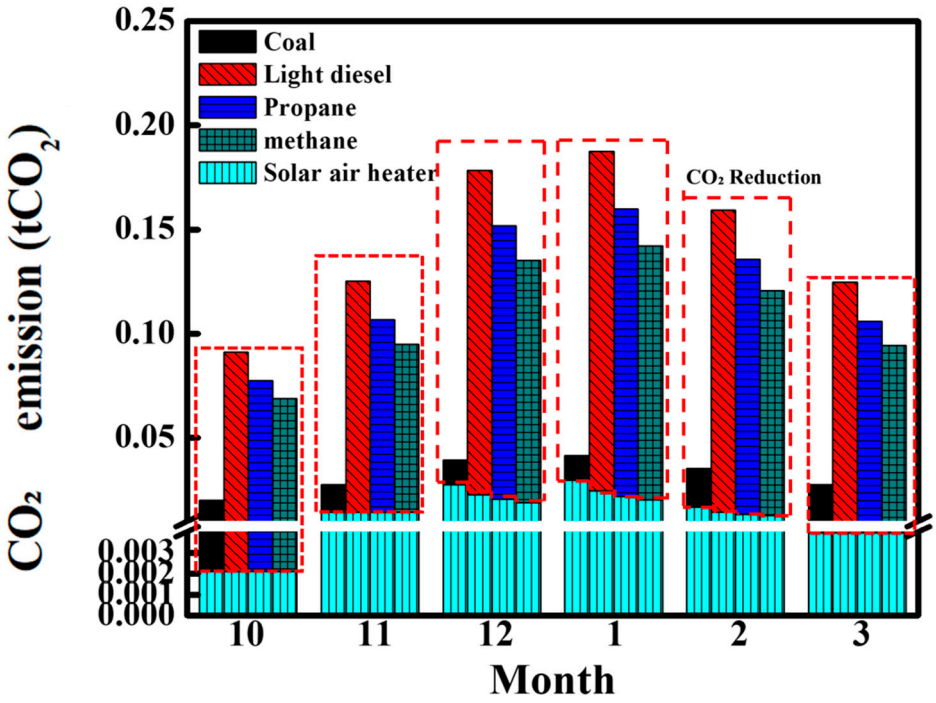

Figure 10. CO_2 generated from a conventional heater by consuming four different fossil fuels. CO_2 reduction achieved with a solar air heater was marked with a red dotted box.

Figure 11 shows the indoor air temperature and tCO_2 changes according to the fan power of the heater in February. Interestingly, by increasing the flow rate of air coming out of the heater, the solar heater can produce enough heat to maintain the target room temperature of 301 K. A fan needs more than 1400 W to power the fan, resulting in CO_2 emission of 0.12 tCO_2. Instead, the heating combined with the conventional heater emits 12 fold less CO_2 emission. The optimal point of the fan power of 100 W where the solar

heater itself could produce the heat for indoor heating in terms of the indoor air temperature of 290.15 K and the lack of heat could be added with a conventional heater with methane as a fuel. Similarly, the best heater operation condition in terms of CO_2 emission could be optimized in December and January. If the heater size is increased, the target room temperature can be maintained in December, January, and February; however, it is not economically reasonable because it is an excess power design in October, November, and March. Based on these results, it can help solve the global warming problem by decreasing the generation of greenhouse gases when using a solar air heater.

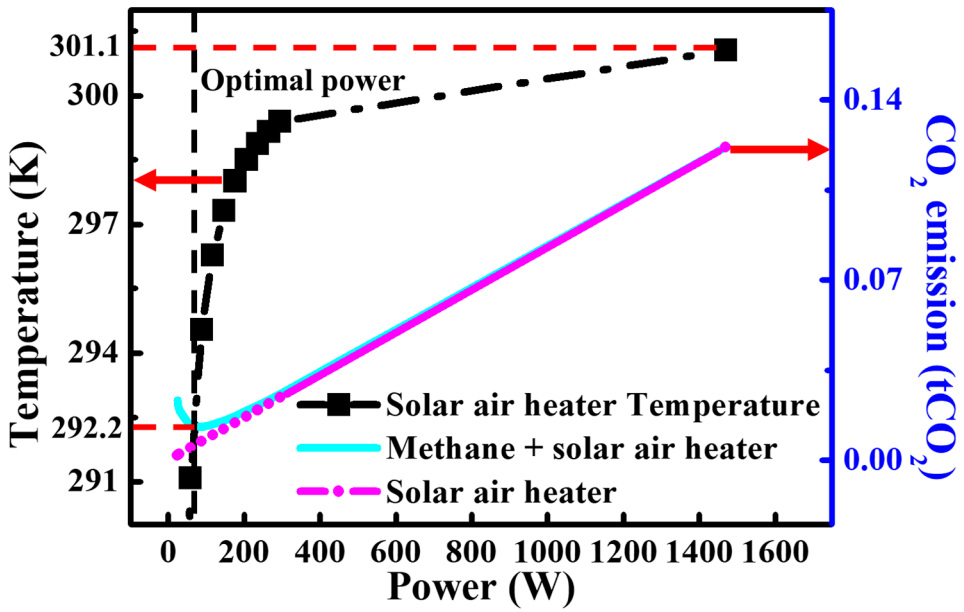

Figure 11. Indoor air temperature and tCO_2 change according to the fan power of the heater in February.

4. Conclusions

A computational model was built to conceive a plan to improve the performance of the solar heater, and experiments were conducted to validate the model. The main results obtained in this study are as follows:

1. Installing the internal structure in the solar heater changes the internal flow characteristic, which induces the air temperature to increase by about 14.2 K on average compared to the heater without the internal structure. This is attributed to enhanced convective heat transfer improved by induced turbulent flow created by the internal structure.
2. The excessive amount of the PCM takes a longer time to be melted such that it causes the air in the solar heater to reach the steady-state temperature (i.e., the maximum temperature). It could even deteriorate the performance of the solar air heater; therefore, the optimal amount of PCM based on the solar irradiance must be determined for the heater to provide warm air for a long time, even at night without the sun.
3. The solar heater designed with an optimal size can reduce the amount of CO_2 generated by about 0.1 tCO_2 on average, which is 0.6 tCO_2 yearly compared to when using conventional heaters only, helping to prevent global warming.

Although this specific result could be applicable in areas with a climate similar to South Korea, this study will be an essential reference for future research and manufacture of more advanced solar heaters. Future research will follow to find the best PCM to perform optimal heater performance.

Author Contributions: Conceptualization, K.K.; methodology, K.K.; software, S.-H.S.; validation, K.K. and J.L.; formal analysis, J.L.; investigation, J.L.; resources, S.-H.S.; data curation, J.L.; writing—original draft preparation, J.L. and S.-H.S.; writing—review and editing, K.K.; visualization, J.L.; supervision, K.K.; project administration, K.K.; funding acquisition, K.K. All authors have read and agreed to the published version of the manuscript.

Funding: This research was funded by the National Research Foundation of Korea (NRF), grant number (2019R1D1A3A03103616).

Institutional Review Board Statement: Not applicable.

Informed Consent Statement: Not applicable.

Data Availability Statement: Not applicable.

Conflicts of Interest: The authors declare no conflict of interest.

Nomenclature

Q	[J/K]	The thermal capacity
m	[kg]	The mass
C_m	[kcal/kgK]	The average of specific heat
C_p	[kcal/kgK]	The mean of specific heat
ρ	[kg/m^3]	Density of the fluid
A	[m^2]	The area of the inlet or outlet
u	[m/s]	The velocity of the fluid
k_{eff}	[W/m^{2}K]	The effective heat transfer coefficient
p	[Pa]	The static pressure
τ_{ij}	[N/m^2]	the shear stress tensor acting on fluids of plane ij
g_i	[m/s^2]	The gravity of species i
μ	[N·s/m^2]	The viscosity of air
G_k	[J]	The kinetic energy of turbulence caused by mean velocity gradient
G_b	[J]	The kinetic energy of turbulence caused by buoyancy
Y_M	[m^{2}K/W]	The effect of fluctuation in the dissipation of turbulence
σ_ε	[/]	The turbulent Prandtl number of ε
σ_k	[/]	The turbulent Prandtl number of k
S_h	[m]	A heat or external energy term produced by a chemical reaction
k_{eff}	[W/m^{2}K]	The effective heat transfer coefficient
$\vec{J}_j$	[m^2/s]	The diffusion flux in paragraph j
t	[sec]	Time
T	[K]	Temperature
Δh	[kJ/kg]	The enthalpy change
F_c	[kg]	The amount of fuel used
H_e	[J]	The amount of heat generated
CO_c	[tC]	The carbon emission quantity
CO_C	[tC/TJ]	The carbon emission coefficient
C_{CO_2}	[tCO$_2$]	The amount of carbon dioxide

References

1. Montaser, M.; Mohamad, R.; Sumsun, N.; Abdul-Ghani, O. The impacts of different heating systems on the environment: A review. *Sci. Total Environ.* **2020**, *766*, 142625.
2. Komilov, O.S.; Sadykov, I.S. Autonomous biogas plant with solar heating system. *J. Innov. Dev. Pharm. Tech. Sci.* **2021**, *4*, 2581–6934.
3. Zeppini, P.; Van Den Bergh, J.C. Global competition dynamics of fossil fuels and renewable energy under climate policies and peak oil: A behavioural model. *Energy Policy* **2020**, *136*, 110907. [CrossRef]
4. Daniel, T.; Zhiyong, T.; Magdalena, B.; Jianhua, F.; Bengt, P.; Simon, F. Large-scale solar thermal systems in leading countries: A review and comparative study of Denmark, China, Germany and Austria. *Appl. Energy* **2020**, *270*, 114997.
5. Potgieter, M.S.W.; Bester, C.R.; Bhamjee, M. Experimental and CFD investigation of a hybrid solar air heater. *Sol. Energy* **2020**, *195*, 413–428. [CrossRef]
6. Ge, T.S.; Wang, R.Z.; Xu, Z.Y.; Pan, Q.W.; Du, S.; Chen, X.M.; Ma, T.; Wu, X.N.; Sun, X.L.; Chen, J.F. Solar heating and cooling: Present and future development. *Renew. Energy* **2017**, *1126*, 1126–1140. [CrossRef]

7. Ahmadi, G.; Toghraie, D.; Akbari, O.A. Solar parallel feed water heating repowering of a steam power plant: A case study in Iran. *Renew. Sustain. Energy Rev.* **2017**, *77*, 474–485. [CrossRef]
8. Chaichan, M.T.; Abass, K.I.; Al-Zubidi, D.S.M.; Kazem, H.A. Practical Investigation of Effectiveness of Direct Solar-Powered Air Heater. *Int. J. Adv. Eng. Manag. Sci.* **2016**, *2*, 1047–1053.
9. Ozgen, F.; Esen, M.; Esen, H. Experimental investigation of thermal performance of a double-flow solar air heater having aluminum cans. *Renew. Energy* **2009**, *34*, 2391–2398. [CrossRef]
10. Khaireldin, F.; Mahamoud, K.; Jalal, F.; Farouk, H.; Cathy, C. A review on phase change materials for thermal energy storage in buildings: Heating and hybrid applications. *J. Energy Storage* **2020**, *33*, 101913.
11. Hamed, M.; Fallah, A.; Brahim, A.B. Numerical analysis of an integrated storage solar heater. *Int. J. Hydrog. Energy* **2017**, *42*, 8721–8732. [CrossRef]
12. Alva, G.; Liu, L.; Huang, X.; Fang, G. Thermal energy storage materials and systems for solar energy applications. *Renew. Sustain. Energy Rev.* **2017**, *68*, 693–706. [CrossRef]
13. Mckenna, P.; Turner, W.J.N.; Finn, D.P. Thermal energy storage using phase change material: Analysis of partial tank charging and discharging on system performance in a building cooling application. *Appl. Therm. Eng.* **2021**, *198*, 117437. [CrossRef]
14. Atalay, A. Assessment of energy and cost analysis of packed bed and phase change material thermal energy storage systems for the solar energy-assisted drying process. *Sol. Energy* **2020**, *198*, 124–138. [CrossRef]
15. Yaomin, C.; Zhixiong, G. Spectral investigation of solar energy absorption and light transmittance in a water-filled prismatic glass louver. *Sol. Energy* **2019**, *179*, 164–173.
16. Kabeel, A.E.; Hamed, M.H.; Omara, Z.M.; Kandeal, A.W. Influence of fin height on the performance of a glazed and bladed entrance single-pass solar air heater. *Sol. Energy* **2018**, *162*, 410–419. [CrossRef]
17. Seyedeh, S.H.; Abas, R.; Ali, A.R. Numerical investigation of natural convection solar air heater with different fins shape. *Renew. Energy* **2017**, *117*, 488–500.
18. Hassan, H.; Abo-Elfadl, S.; El-Dosoky, M.F. An experimental investigation of the performance of new design of solar air heater (tubular). *Renew. Energy* **2020**, *151*, 1055–1066. [CrossRef]
19. Mehrdad, M.; Ali, H.; Somchai, W. Geometry optimization of double pass solar air heater with helical flow path. *Sol. Energy* **2021**, *213*, 67–80.
20. Alam, T.; Kim, M.H. Performance improvement of double-pass solar air heater—A state of art of review. *Renew. Sustain. Energy Rev.* **2017**, *79*, 779–793. [CrossRef]
21. Ali, H.; Mehrdad, M. Experimental analysis and numerical modeling of solar air heater with helical flow path. *Sol. Energy* **2018**, *162*, 278–288.
22. Rashidi, S.; Javadi, P.; Esfahani, J.A. Second law of thermodynamics analysis for nanofluid turbulent flow inside a solar heater with the ribbed absorber plate. *J. Therm. Anal. Calorim.* **2019**, *135*, 551–563. [CrossRef]
23. Rajneesh, K.; Anoop, K.; Varun, G. A parametric analysis of rectangular rib roughened triangular duct solar air heater using computational fluid dynamics. *Sol. Energy* **2017**, *157*, 1095–1107.
24. Jouybari, N.F.; Lundström, T.S. Performance improvement of a solar air heater by covering the absorber plate with a thin porous material. *Energy* **2020**, *190*, 116437. [CrossRef]
25. Singh, A.P.; Singh, O.P. Performance enhancement of a curved solar air heater using CFD. *Sol. Energy* **2018**, *174*, 556–569. [CrossRef]
26. Kim, K.B.; Choi, K.W.; Kim, Y.J.; Lee, K.H.; Lee, K.S. Feasibility study on a novel cooling technique using a phase change material in an automotive engine. *Energy* **2010**, *35*, 478–484. [CrossRef]
27. The Intergovernmental Panel on Climate Change (IPCC). Available online: https://www.ipcc.ch (accessed on 28 June 2021).
28. Ukrainczyk, N.; Kurajica, S.; Šipušić, J. Thermophysical Comparison of Five Commercial Paraffin Waxesas Latent Heat Storage Materials. *Chem. Biochem. Eng. Q.* **2009**, *24*, 129–137.
29. Dai, B.; Qi, H.; Liu, S.; Zhong, Z.; Li, H.; Song, M.; Ma, M.; Sun, Z. Environmental and economical analyses of transcritical CO_2 heat pump combined with direct dedicated mechanical subcooling (DMS) for space heating in China. *Energy Convers. Manag.* **2019**, *198*, 111317. [CrossRef]
30. International Energy Agency (IEA). Available online: https://www.iea.org (accessed on 28 June 2021).